

Finite Element Modeling of Deformation Behavior of Steel Specimens under Various Loading Scenarios

Dilip Banerjee^{1,a*}, Mark Iadicola^{1,b}, Adam Creuziger^{1,c}, and Timothy Foecke^{1,d}

¹Material Measurement Laboratory, NIST, 100 Bureau Dr, Gaithersburg, MD 20899, USA

^aDilip.Banerjee@nist.gov, ^bMark.Iadicola@nist.gov, ^cAdam.Creuziger@nist.gov,

^dTimothy.Foecke@nist.gov

Keywords: uniaxial and biaxial tensile tests, finite element modeling, steel, cruciform

Abstract. Lightweighting materials (e.g., advanced high strength steels, aluminum alloys etc.) are increasingly being used by automotive companies as sheet metal components. However, accurate material models are needed for wider adoption. These constitutive material data are often developed by applying biaxial strain paths with cross-shaped (cruciform) specimens. Optimizing the design of specimens is a major goal in which finite element (FE) analysis can play a major role. However, verification of FE models is necessary. Calibrating models against uniaxial tensile tests is a logical first step. In the present study, reliable stress-strain data up to failure are developed by using digital image correlation (DIC) technique for strain measurement and X-ray techniques and/or force data for stress measurement. Such data are used to model the deformation behavior in uniaxial and biaxial tensile specimens. Model predictions of strains and displacements are compared with experimental data. The role of imperfections on necking behavior in FE modeling results of uniaxial tests is discussed. Computed results of deformation, strain profile, and von Mises plastic strain agree with measured values along critical paths in the cruciform specimens. Such a calibrated FE model can be used to obtain an optimum cruciform specimen design.

1. Introduction

Automotive companies are actively interested in the increased use of advanced lightweighting materials such as advanced high strength steels (AHSS), aluminum alloys etc. as sheet metal components. However, accurate material models are needed before these materials can be widely used. These material models are often developed using linear strain paths using cross-shaped biaxial specimens (i.e., cruciform) [1, 2, 3]. But successful cruciform mechanical testing is dependent on the specimen design itself. In the past, a wide variety of designs have been used [4, 5, 6, 7]. The specimen design should meet certain goals: (a) Both strain uniformity and eventual failure in the biaxially loaded gauge area, (b) reduction of stress concentration outside of the gauge area, (c) minimization of shear strains in the gauge area, and (d) similar behavior during repeat tests. A prudent approach for obtaining optimum specimen design is to combine FE simulation with optimization software such that the above objectives are achieved. But the first step is to calibrate the FE model against precise experimental measurements. These measurements were obtained using the state of the art mechanical testing facility at the National Institute of Standards and Technology (NIST) Center for Automotive Lightweighting (NCAL) [8]. In this paper, the verification of FE models against experimental measurements is discussed for both uniaxial and biaxial tensile tests. Additionally, plastic deformation behavior in the specimens is discussed. Note that uncertainties associated with the measurement of displacement and strain are reported in ref [9].

2. Uniaxial Tensile Tests

2.1 Uniaxial Tensile Test Experiments. Uniaxial test specimens were made of two different steels: (a) 9.525 mm (0.375 in) thick hot-rolled low carbon steel (hereinafter called “thick specimen”) and (b) 3.038 mm (0.1196 in) thick cold-rolled AISI 1008 steel (hereinafter called “thin specimen”). This thin specimen steel has much lower yield and ultimate tensile strength than the thick specimen

steel. Uniaxial tests were conducted both to verify the FE model and to generate stress-strain data for uniaxial and biaxial tensile tests. Uniaxial tensile tests were performed for both steels in the rolling direction of the sheet. These tests were performed using the X-axis of the cruciform machine and the DIC system [8]. The gauge section as designed has a nominally parallel length of 101.6 mm and width of 19.05 mm with radii of 50.8 mm to the 28.58 mm wide end-tabs. The same planar geometry was used for both thicknesses of material. Since the biaxial test and model will

achieve strains beyond the uniform strain of a standard tensile test, it was necessary to approximate the true-stress/true-strain relationship at strains beyond uniform deformation. The true axial strain was calculated as the average strain across the width for each point in time in the axial direction at the eventual location of failure. The true stress was calculated as the applied force divided by the current cross-sectional area at the same location and time. The resulting stress strain curves are shown in Fig. 1. The uniaxial test for the thin material

Fig. 1. True stress – true strain data obtained in uniaxial tensile tests.

used a constant displacement rate, which resulted in an undesirable increase in strain rate from approximately $8 \times 10^{-5} \text{ s}^{-1}$ before initial localization (maximum force) to $2 \times 10^{-3} \text{ s}^{-1}$ as the sample approached failure. In the thick material uniaxial test the displacement rate was reduced twice during the test (at approximately 0.26 and 0.49 true strain) to keep the average strain rate near $9 \times 10^{-4} \text{ s}^{-1}$. Following the tensile tests, history-dependent axial displacement values at locations in the end-tabs approximately 82 mm away from the central point were extracted for subsequent use in the FE simulation as boundary conditions (BC). The displacement values were interpolated from the DIC field data at the FE nodal coordinate values nearest to $X = \pm 82 \text{ mm}$ along the axial direction. The force-displacement curve for the thick specimen is shown in Fig. 2. Displacement and strain data corresponding to the four loading points (A, B, C, and D) in Fig. 2 were extracted for

comparison with FE results. Such axial displacement vs. x-coordinate data as measured by the DIC system were output along three specimen lines (i.e., along centerline, along lines $\pm 4.63 \text{ mm}$ away from centerline) in the axial direction. Only centerline data are used in this study.

2.2 FE Simulation of Uniaxial Tensile Tests.

A 3D finite element model of the thick uniaxial specimen was developed using ABAQUS¹ software [10]. Constitutive material model data were obtained from experimental stress-strain

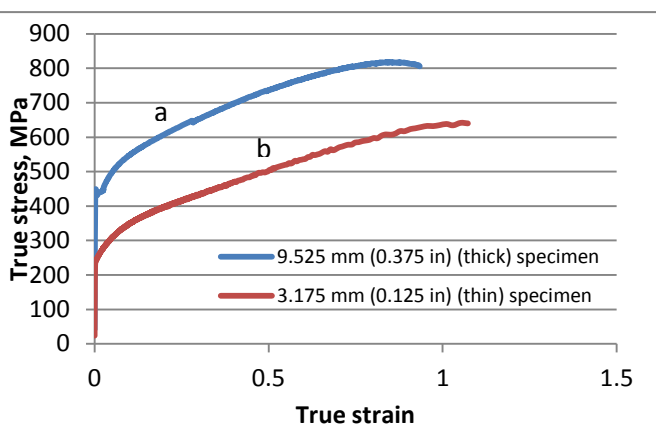


Fig. 1. True stress – true strain data obtained in uniaxial tensile tests.

used a constant displacement rate, which resulted in an undesirable increase in strain rate from approximately $8 \times 10^{-5} \text{ s}^{-1}$ before initial localization (maximum force) to $2 \times 10^{-3} \text{ s}^{-1}$ as the sample approached failure. In the thick material uniaxial test the displacement rate was reduced twice during the test (at approximately 0.26 and 0.49 true strain) to keep the average strain rate near $9 \times 10^{-4} \text{ s}^{-1}$. Following the tensile tests, history-dependent axial displacement values at locations in the end-tabs approximately 82 mm away from the central point were extracted for subsequent use in the FE simulation as boundary conditions (BC). The displacement values were interpolated from the DIC field data at the FE nodal coordinate values nearest to $X = \pm 82 \text{ mm}$ along the axial direction. The force-displacement curve for the thick specimen is shown in Fig. 2. Displacement and strain data corresponding to the four loading points (A, B, C, and D) in Fig. 2 were extracted for

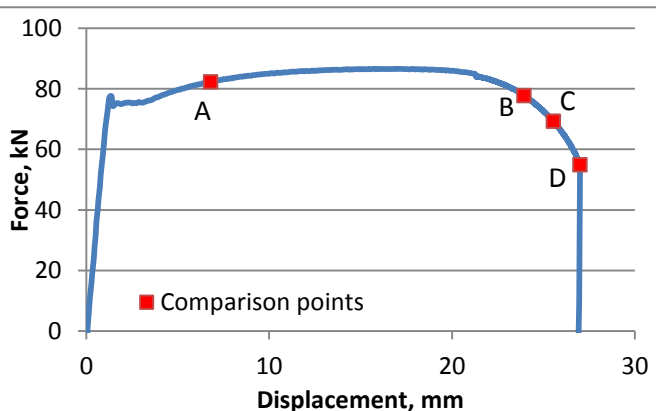


Fig. 2. Force-displacement curves for the thick specimen.

¹ Certain commercial software or materials are identified to describe a procedure or concept adequately. Such identification is not intended to imply recommendation, endorsement, or implication by NIST that the software or materials are necessarily the best available for the purpose.

data in uniaxial tension tests (Fig. 1). Isotropic hardening is assumed in this study. Young's modulus of 210 GPa and Poisson ratio of 0.3 were assumed for both materials. A 1/2 symmetry FE

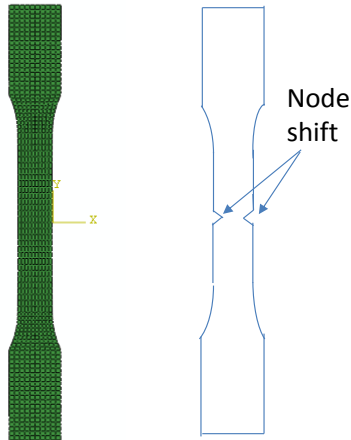


Fig. 3. Finite element mesh and a schematic showing node shift used to introduce instability in FE

model was developed by taking advantage of the mirror symmetry in the specimen shape and loading. The solid model was developed using mapped meshing, and 3D linear hexahedral elements (C3D8R) were used. Fig. 3 shows a typical FE mesh. In order to introduce instability in the simulation, geometric imperfections were introduced. This was accomplished by physically displacing nodes at the edge by a small fraction of the grid spacing (see Fig. 3). Note that all the nodes through the depth at this edge location were displaced by the same amount. This is similar to the concept of creating a notch to initiate instability. ABAQUS simulations showed that the ultimate failure occurred near the vicinity of this imperfection but not at the exact point of imperfection. Experiments on the thick specimens showed the formation of Lüders bands (typically

encountered in low carbon steels). The eventual necking and failure occurred near the locations where Lüders bands initiated. Therefore, it was necessary to capture this behavior in the FE simulation by introducing imperfections near the regions where the Lüders bands were seen.

Figure 4 shows both the measured and computed axial displacements along the centerline of the specimen for points corresponding D in Fig. 2. Good agreement was seen except for the point near the necking region. This is because there is a slight difference between the model predicted location of necking and that obtained in the experiment. Additionally, the model seems to predict a sharper localization than that seen in the experimental results. Figure 5 shows the comparison between the measured von Mises equivalent strain and computed von Mises plastic strain plots. Again, the agreement is good in terms of the overall shape and maximum values. However, ABAQUS values slightly under-predict the strains away from the maximum localization point. This is understandable, as ABAQUS plots do not include the elastic component of the strain (which is quite small compared to the plastic component of the strain). Figure 6 shows measured and computed contour plots of von Mises equivalent strain on the surface of the specimen. The overall strain profile along the specimen length as computed by ABAQUS agrees well with measured values.

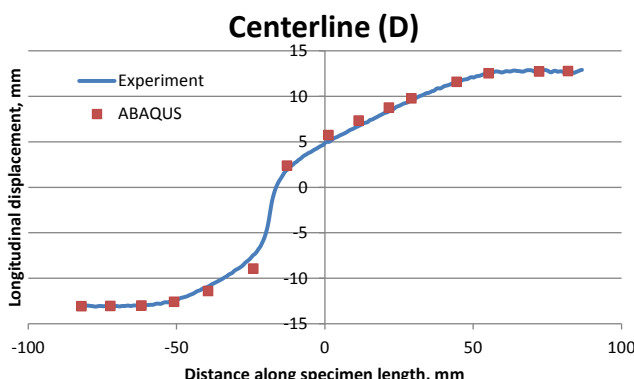


Fig. 4. Measured and computed longitudinal displacements along the specimen length corresponding to the point D in Fig. 2.

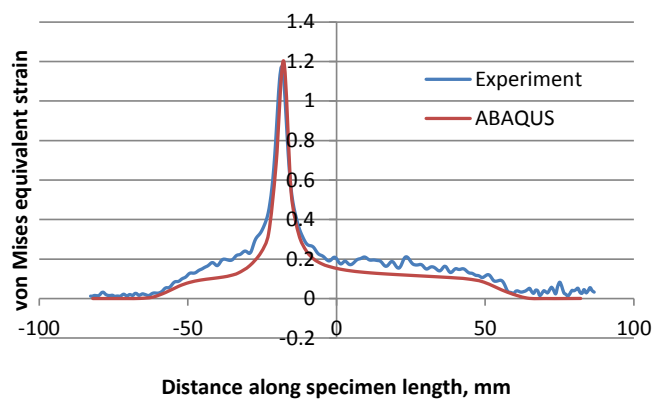


Fig. 5. von Mises equivalent strain and ABAQUS computed von Mises plastic strain along the specimen length corresponding to point D in Fig. 2.

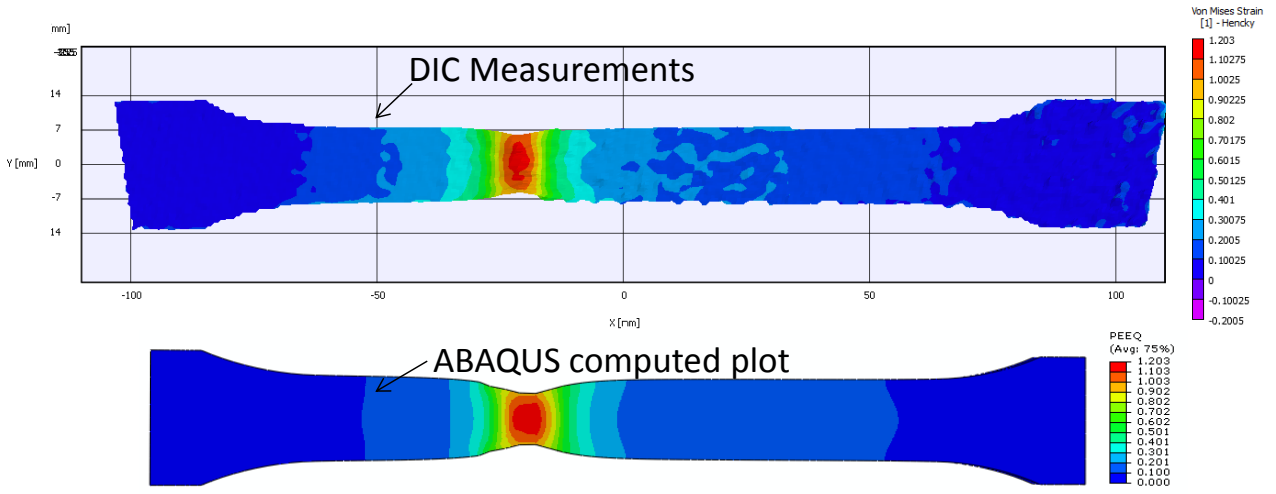


Fig. 6. Contour plots of measured von Mises equivalent strain and ABAQUS computed von Mises plastic strain along the specimen length corresponding to point D in Fig. 2.

3. Biaxial Tensile Tests

3.1 Cruciform Specimen Design. Cruciform geometries for in-plane biaxial tests are advantageous because (a) the region of interest is far away from locations where BCs are applied and (b) varying strain ratios can be applied along the arms of the specimen. In most of the specimen designs, failure occurred outside the central gauge section of interest and at strains well below traditional forming limit strains, due to a combination of various factors such as stress and deformation concentrations at corners or near slits in the arms [11]. In some designs, the central gauge section is thinned down to achieve higher strain and possibly failure in the middle of the gauge section. In this study, the specimen design follows that of ref. [7], with the initial specimen being enlarged in all three directions to a thickness of 0.953 mm. The present specimen design for the thick specimen is described in ref [9]. Cruciform samples were machined by water-jet with the X-axis aligned with the rolling direction of the sheet. A similar geometry was used for the thin specimen, except that it had a designed thickness of 0.749 mm (0.0295 in) in the thinned down region in the center and that the fillet radius at the peripheral region of the central pocket was 0.397 mm (0.016 in).

3.2 Biaxial Tensile Tests. Biaxial loading was applied using four hydraulic actuators, which are controlled in orthogonal pairs [11]. Each of these actuators has 500 kN load capacity and has a ± 50 mm displacement range from a reference distance of 640 mm between grip faces on the X or Y-axis. Details of the loading and in situ DIC data acquisition are described in [11]. In the present study, the biaxial tests were conducted using displacement control. Fig. 7 shows force-displacement curves. The 3D displacement of top surface about the center of the cruciform specimen was measured with a stereo DIC system. Surface strains are calculated from the measured displacement fields. Measured, history-dependent average U and V values at locations approximately 25 mm away from the central point were extracted for subsequent use in FE simulation (see Fig. 8). Since cruciform specimens tend to concentrate strain in the corners between the arms leading to premature failure, it is important for FE model to be able to capture the mechanical behavior in these corners. Accordingly, measured displacement and strain data were extracted along a diagonal line that bisects the region between the central pocket and the reentrant radius at the meeting point of the X and Y arms (see "Path" in Fig. 8). These data are compared to FE data corresponding to loading points shown in Fig. 7. Results are shown here for only the maximum force point in Fig. 7.

3.3 FE Modeling. A 3D FE model of the cruciform specimens was developed using ABAQUS software [10]. See section 2.2 for details on material data. A 1/8th symmetry model was developed

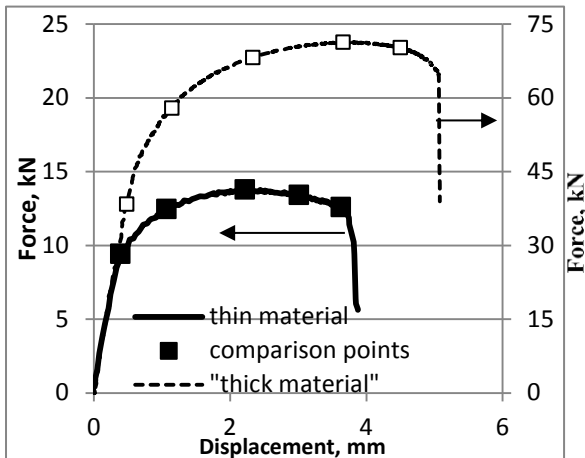


Fig. 7. Force-displacement curves for X-axis from cruciform specimens.

by using the mirror symmetry in the specimen shape and loading. FE model included both regular (C3D8) and reduced integration brick (C3D8R) elements. In addition to symmetry conditions, axial displacement boundary conditions were applied on each arm (Fig. 8). Simulated results were extracted for all points labeled in Fig. 7 along the path shown in Fig. 8 and compared with DIC data. Only data corresponding to the maximum force point are discussed below for the thin specimen.

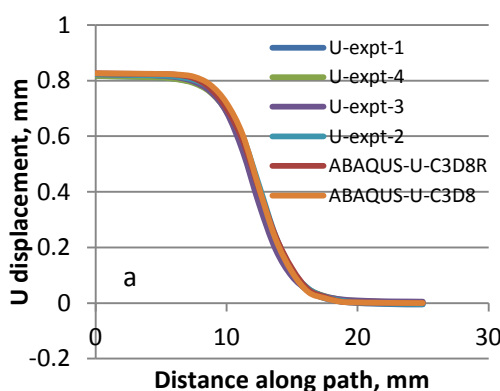


Fig. 9. U displacement along path in Fig. 8: U-expt-1 etc. (measured); ABAQUS-U-C3D8 etc. (computed).

e_{zz} for C3D8 element exceeds those seen in experimental data. It is also noticed that the model predicts a slightly narrower width of the e_{zz} profile than that in the experimental results. The measured von Mises equivalent strain plot is shown in Fig. 11. This plot is compared with the von Mises equivalent plastic strain (PEEQ) in ABAQUS. This comparison is justified since elastic strain is very small. Fig. 11 shows the largest value at the reentrant radius of about 0.38 and around 0.084 in the central region. Uniform equivalent strain is seen in the central pocket, which is also seen in the ABAQUS results in Fig. 12. The ABAQUS results show a value of 0.16 in the central pocket and a value of 0.3 at the outer edge of the reentrant corner. The model shows a slight decrease in strain along the diagonal from the reentrant radius to the peripheral region of the central pocket, where a value of about 0.24 is obtained. Although the model does not show as thick a band of PEEQ of 0.3 along the diagonal from the reentrant radius to the peripheral region of the central pocket (as seen in experimental result in Fig. 11), it is intuitive that the failure initiation will probably start at the strain concentration at the base of the fillet from the thicker region into the thinner region. In fact, the experiment showed that the failure initiated at both the top left and

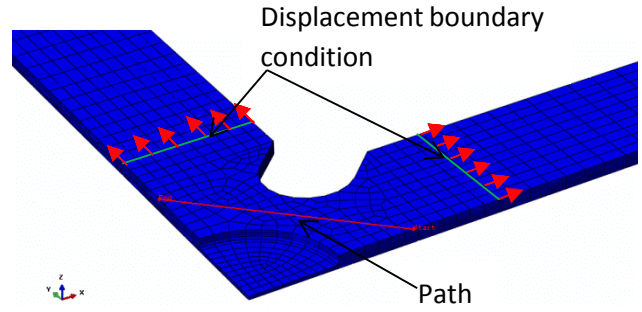


Fig. 8. A portion of the FE mesh of the thin cruciform specimen along with locations for axial displacement boundary conditions. Also shown is the path on which the FEA results are extracted for comparison with experimental measurements.

3.4 Results and Discussion. Fig. 9 shows both experimental and computed U displacement fields. There are four equivalent paths for which experimental data have been measured. However, because of the symmetry used in the model, only one plot is available for the FE model. Two sets of ABAQUS results are shown (one each for C3D8R and C3D8 element). Fig. 9 shows that the model predicts the displacement field correctly. Fig. 10 shows plots of normal strains in the Z direction. The measured thickness strains were calculated assuming volume conservation, using $e_{zz} = -(e_{xx} + e_{yy})$. ABAQUS simulations with C3D8 elements are in better agreement with experimental results. However, the modeled peak

value of e_{zz} for C3D8 element exceeds those seen in experimental data. It is also noticed that the model predicts a slightly narrower width of the e_{zz} profile than that in the experimental results. The measured von Mises equivalent strain plot is shown in Fig. 11. This plot is compared with the von Mises equivalent plastic strain (PEEQ) in ABAQUS. This comparison is justified since elastic strain is very small. Fig. 11 shows the largest value at the reentrant radius of about 0.38 and around 0.084 in the central region. Uniform equivalent strain is seen in the central pocket, which is also seen in the ABAQUS results in Fig. 12. The ABAQUS results show a value of 0.16 in the central pocket and a value of 0.3 at the outer edge of the reentrant corner. The model shows a slight decrease in strain along the diagonal from the reentrant radius to the peripheral region of the central pocket, where a value of about 0.24 is obtained. Although the model does not show as thick a band of PEEQ of 0.3 along the diagonal from the reentrant radius to the peripheral region of the central pocket (as seen in experimental result in Fig. 11), it is intuitive that the failure initiation will probably start at the strain concentration at the base of the fillet from the thicker region into the thinner region. In fact, the experiment showed that the failure initiated at both the top left and

bottom right of the pocket area at the base of the fillet radius, and these cracks propagated from the periphery to the center of the pocket.

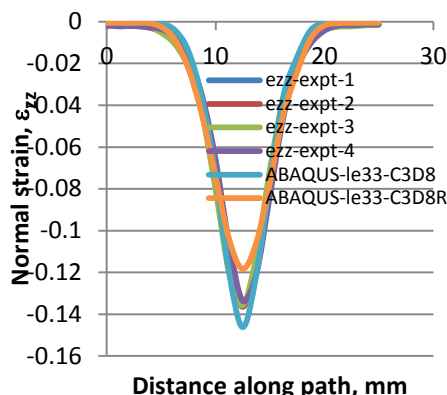


Fig. 10. Z normal strains: ezz-expt-1 etc.
(measured); ABAQUS-le11-C3D8R (ABAQUS).

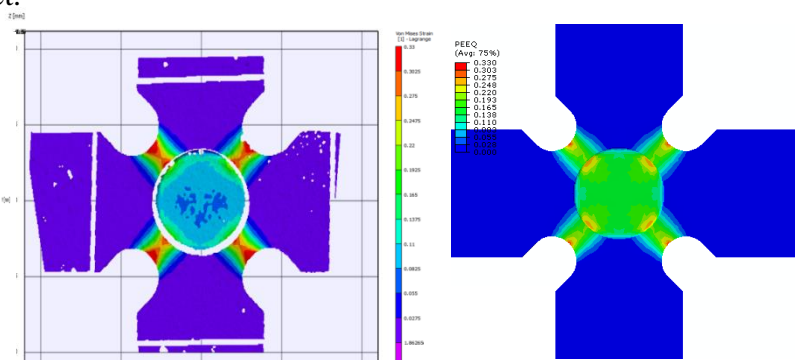


Fig. 11. Measured von Mises strain.

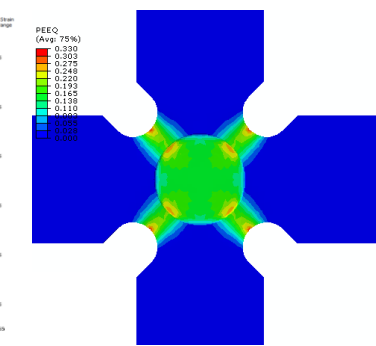


Fig. 12. ABAQUS computed von Mises equivalent plastic strain using C3D8 elements.

4. Summary

FE analyses of uniaxial and biaxial tensile tests were conducted using ABAQUS software. The numerical model uses constitutive material data obtained in uniaxial tests. The model employed history-dependent displacement BC data that were obtained from in situ DIC measurements. Overall, the numerical model showed reasonable agreement with experimental measurements. The model predicted the necking correctly in uniaxial specimen. Biaxial straining were seen in the central region of interest in cruciform, as desired. The model predicts the path along which the eventual failure was seen in the experiment. This model can be used for specimen optimization.

5. References

- [1] T. Foecke et al., A method for direct measurement of multiaxial stress-strain curves in sheet metal, *Mater Trans.* 38A (2007) 306–313.
- [2] M.A. Iadicola, T. Foecke, S.W. Banovic, Experimental observations of evolving yield loci in biaxially strained AA 5754-O, *Int. J. Plasticity.* 24(2008) 2084–2101.
- [3] W. Müller, K. Pöhlandt, New experiments for determining yield loci of sheet metal, *J. Mater. Process. Tech.* 60 (1996) 643–648.
- [4] C.C. Tasan et al., In-Plane biaxial loading of sheet metal until fracture, Society for Experimental Mechanics (SEM), Orlando, FL, 2008.
- [5] E. Hoferlin et al., The design of a biaxial tensile test and its use for the validation of crystallographic yield loci, *Model. Simul. Mater. Sc.* 8 (2000) 423–433.
- [6] T. Kuwabara, A. Bael, E. Iizuka, Measurement and analysis of yield locus and work hardening characteristics of steel sheets with different r-values, *Acta Mater.* 50 (2002) 3717–3729.
- [7] F. Abu-Farha, L.G. Hector, M. Khraisheh, Cruciform-shaped specimens for elevated temperature biaxial testing of lightweight materials, *JOM* 61 (2009) 48–56.
- [8] NIST Center for Automotive Lightweighting, <http://www.nist.gov/lightweighting/>.
- [9] D. Banerjee, M. Iadicola, A. Creuziger, T. Foecke, An Experimental and Numerical Study of Deformation Behavior of Steels in Biaxial Tensile Tests, to be published in TMS 2015 Conference Proceedings, Warrendale, PA.
- [10] ABAQUS 12.2 software. Dassault Systemes. <http://www.3ds.com/>.
- [11] M.A. Iadicola, A.A. Creuziger, T. Foecke, Advanced biaxial cruciform testing at the NIST Center for Automotive Lightweighting, SEM , 2013.